International Research Journal of Multidisciplinary Scope (IRJMS), 2026;7(3):1091-1108

Original Article | ISSN (O): 2582-631X DOI: 10.47857/irjms.2026.v07i03.012212

Seeing Through Darkness: Fusion of Optical and Thermal Features for Improved Space Object Classification

Sunita Jahirabadkar[1]*, Raahi Kadu[1], Sai Gokhale[1], Grishma Deshmukh[1], Sejal Chaudhari[1], Aditya R[2]

[1]Department of Computer Engineering, Cummins College of Engineering for Women, Pune, Maharashtra, India, [2]U. R. Rao Satellite Center (URSC), Indian Space Research Organization (ISRO), Bengaluru, Karnataka, India. *Corresponding Author's Email: sunita.jahirabadkar@cumminscollege.in

Abstract

In recent years, the growing amount of space debris has posed a significant threat to space operations. On-orbit visual sensors used to detect space debris have emerged as a promising solution for maintaining spacecraft safety. However, the performance of visual sensors is highly dependent on illumination, which is often insufficient under low-light conditions. Since visible and thermal images complement each other effectively in such environments, a visible and thermal image fusion technique is utilized to enhance the application of visual sensors. A dataset containing recorded visible and thermal images of space debris was developed for model validation. This paper presents a novel approach for the fusion of visible and thermal images, followed by the classification of the fused images into space debris or satellites. The fused images are then fed into a classifier to distinguish between space debris and satellites. Experimental results are compared using different classification algorithms to identify the most effective algorithm for achieving better performance. The proposed approach shows promise for the accurate identification and categorization of objects in space. Future work will focus on improving real-time implementation, expanding the dataset to include diverse orbital scenarios and exploring advanced deep learning models to further enhance detection accuracy. Additionally, the motion of space objects may be incorporated into the classification process, using video fusion techniques.

Keywords: Deep Learning, Image Classification, Image Fusion, Space Debris, Thermal Imaging.

Introduction

Space debris, also known as space junk, has emerged as a critical issue in modern space exploration. With decades of space missions and satellite launches, Earth's orbit has become cluttered with discarded rocket stages, defunct satellites and fragments from past space activities. These debris particles pose a significant risk to functioning satellites, spacecraft and even human life. The exponential proliferation of space debris presents major challenges to future space missions and the long-term sustainability of space activities. Effective detection, monitoring and categorization of space debris are therefore essential for ensuring the safety and sustainability of space-based operations (1). In this context, this research proposes a fusion and classification technique that utilizes visible and thermal images to accurately distinguish between space debris and operational satellites. Image fusion combines information from multiple images into a single, more informative image, enhancing perception and analysis. It integrates complementary data from different sensors, overcoming the limitations of individual viewpoints. A widely used application is visible–thermal image fusion, which merges visual and thermal information for improved interpretation and subsequent processing tasks (2). Visible images capture detailed texture, edges and spatial features, making them highly suitable for human perception. However, their performance degrades under poor illumination, limiting object detection in dark regions. Thermal imaging complements visible imaging by detecting heat signatures, enabling reliable observation when visible sensors are ineffective. Together, visible and thermal cameras provide complementary information for dynamic environments (3). Thermal imaging captures the infrared radiation emitted by objects, enabling the visualization of temperature variations and heat signatures.

(Received 07th April 2026; Accepted 17th June 2026; Published 18th July 2026

This information enhances the capability to detect and identify objects, especially under challenging conditions such as low light, adverse weather, or camouflage. In scenarios where the visible characteristics of space debris and satellites are difficult for a model to distinguish, such as in the case of defunct satellites categorized as debris, thermal properties play a crucial role. Satellites generally maintain a controlled temperature, whereas space debris exhibits varying temperatures depending on the surrounding environment. Typically, debris can be identified by its relatively lower temperature (4).

By fusing visible and thermal images, the resulting composite image combines the visual details of the visible spectrum with the thermal characteristics of objects. This fusion enables improved object recognition, enhanced target discrimination and greater situational awareness in applications such as surveillance, security and search and rescue. The integration of visible and thermal imagery provides a more comprehensive understanding of the scene, thereby supporting improved decision-making and analysis in complex scenarios.

Many articles are available in the literature presenting their research on the detection, identification and categorization of space debris using various imaging technologies and machine learning techniques. The importance of thermal imaging instruments in characterizing space debris has been emphasized in the literature (5). The researchers have highlighted the significance of thermal imaging in understanding debris behavior, properties and thermal signatures. A Blender-based diversified space target dataset incorporating multiple debris types and a realistic on-orbit environment has been developed (6). This dataset specifically focuses on visible spectrum images and is beneficial for researchers working on space debris detection systems. An approach for detecting space debris was proposed that incorporates pre-processing techniques to remove background noise and hot pixels. Furthermore, a novel method for detecting space debris in optical image sequences using Feature Learning of Candidate Regions (FLCR) was proposed. They also proposed a method for removing hot pixels and effectively eliminating background noise through a one-iteration approach based on a Gaussian Mixture Model (GMM) (7).

The detection and identification of objects in orbit have been addressed using machine learning techniques. By combining deep learning techniques with computer vision methodologies, the study achieves a high classification accuracy of 98.9% (8). Gaussian Mixture Models (GMMs) have been utilized to distinguish between foreground and background elements, achieving an accuracy of 92.5% (9). YOLO (You Only Look Once) models have also been proposed for object recognition in thermal images and videos captured by Unmanned Aerial Vehicles (UAVs). The study involves annotating images obtained from a drone-mounted thermal camera to facilitate object classification (10).

A Deep Convolutional Neural Network (DCNN) model for space target detection was developed by the researchers. By selecting optimal data, the model achieves excellent classification accuracy of 99.90%. The issue of noisy and ambiguous images in satellite and debris categorization is addressed by researchers, who generated mask images from RGB photographs, which are then fed into a Convolutional Neural Network (CNN) for efficient classification, achieving an accuracy of 97.7% (11). A multimodal deep learning approach combining RGB and depth information was evaluated on the SPARK dataset for the recognition of spacecraft and debris. By incorporating depth information as an additional channel, the study achieves an accuracy of 85% in classification tests (12). An image-based simulator along with a feature extraction model based on PointNet is used to detect satellites (13).

These research papers highlight the application of various imaging technologies and machine learning techniques for space debris detection, identification and classification. They emphasize the importance of reliable data generation, pre-processing techniques, deep learning models and multimodal approaches in improving the understanding and management of space debris. Based on these findings, a novel visible–thermal image fusion algorithm is proposed for classifying space resident objects.

Methodology

The methodology section presents a comprehensive approach to this study, beginning with data creation. In Workflow 1, an accurate experimental setup was established to capture visible and thermal images. Workflow 2 utilized Blender to simulate realistic 3D image sequences, thereby enhancing the diversity and complexity of the dataset. Prior to analysis, a crucial image registration step was implemented for the data generated using Workflow 1 to ensure proper image alignment.

An innovative image fusion technique was then employed to combine thermal and optical image sequences, enabling the extraction of comprehensive features for accurate classification and enriching the data with robust and meaningful information. In the final phase of image classification, advanced algorithms and deep learning models were deployed to categorize space objects as either satellites or debris, thereby facilitating efficient and reliable onboard detection. The seamless integration of these methodological components ensured reliable and robust findings, significantly contributing to optical image-based space debris detection.

Dataset Creation

The current datasets developed for Space Debris Detection, like SPARK, STAR24K and a few others do not include thermal modality for space objects (14, 15). The proposed approach is data-scarce and hence necessitates the creation of a dataset including thermal and visible image modalities. The dataset creation module is divided into two separate workflows which were implemented parallelly. The dataset which provided desirable outputs was used for the subsequent modules, i.e., image fusion and image classification. Workflow-1 uses an experimental setup of 3D Space Object models and a camera with thermal and visible spectrum lenses for data creation. Workflow-2 consists of the simulation of Space Objects on the Blender software to render animations and create a dataset of visible and thermal images. The limitation of workflow 1 involved improper mapping of the 2 images while fusion since the camera lenses had an offset. Although, this could be overcome using image registration techniques later, it necessitated a parallel workflow 2 of model simulation in Blender. Workflow 2 is a more refined approach that addresses the limitations of its predecessor. This workflow incorporates advanced data collection and quality assurance measures, ensuring a more accurate and comprehensive dataset for our analysis needs.

Workflow 1

Experimental Setup: The process of data creation entails capturing images from an experimental space setup using a camera with thermal and visible spectrum lenses and a 3D space simulation setup. The workflow involves an experimental setup in a dark room to simulate the illumination conditions of the space environment, as shown in Figure 1.

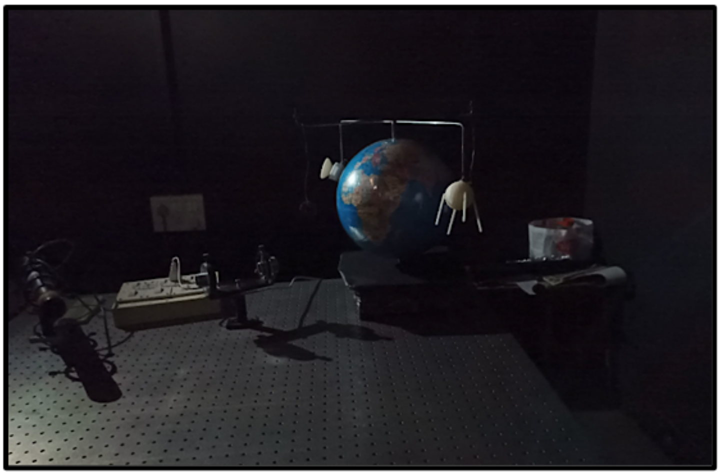

Figure 1: Experimental Setup

Detecting whether the object is debris or a satellite in a dark environment or in the absence of sunlight is a crucial task. Based on the experiments by various researchers, it has been observed that this task is relatively easy in the presence of sunlight, but additional complexity is added when we try to detect the objects in darkness. Researchers have tried generating the data using visual cameras (16, 17). However, there is no data available in the literature, captured using a thermal camera. In this experimental setup, a novel data capturing technique is used for capturing the data which may lead to the accurate classification of the objects to a satellite or debris using thermal as well as visual imaging.

This process involved the following tasks: Darkroom creation, Object creation using 3-D printing and capturing images in the presence of light and in dark mode using visible and thermal cameras simultaneously.

Figure 1 details the setup created for our own Satellite and Debris image collection in a dark room. The process included the collection of videos of debris and satellites at different temperatures, locations and light conditions, as well as the capture of thermal and visible images using a real-time camera in simulated space scenarios.

The setup uses satellites and debris models created by the 3-D printer, as shown in Figures 2A and 2B. The 3-D model of SAT1 (Satellite 1) is shown in Figure 2A and the model of Sputnik Satellite is shown in Figure 2B. The temperatures of these objects were changed by heating them and cooling them up to a range of -20°C to 80°C to simulate their thermal properties in space environment conditions. CREO software is used to create satellite models. Satellite model 1 (SAT1) is created with a 5 cm X 5 cm cube, with solar plates that are 5 cm wide. Satellite model 2 is designed as a Sputnik with a 5 cm diameter and legs that are 1 mm wide. The satellite 3-D CAD model is 3-D printed in the laboratory. The material used to create the 3-D print of the satellite model is PLA (Polylactic Acid). The 3-D-printed object can withstand a maximum temperature of up to 215^{0}C. Also, other available materials are ABS (Acrylo-nitrile butadiene styrene) and Carbon fibre for 3-D printing.

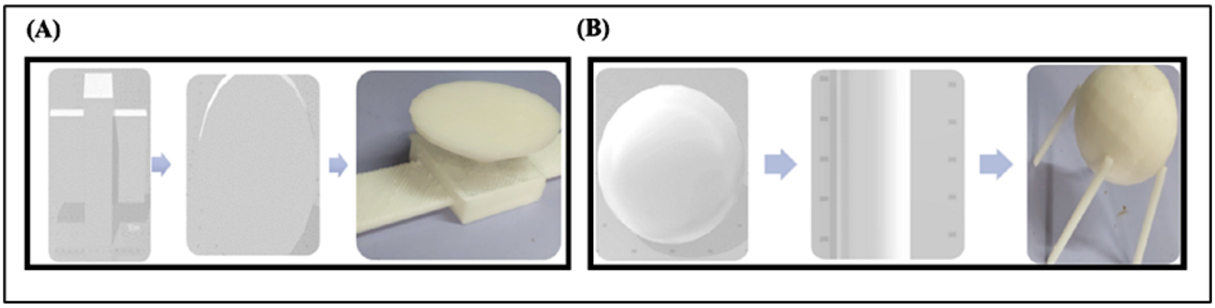

Figure 2: 3-D Printed Models of Satellites. (A) 3-D Printed Model of SAT1 (Satellite1), (B) 3-D Printed Model of Sputnik Satellite

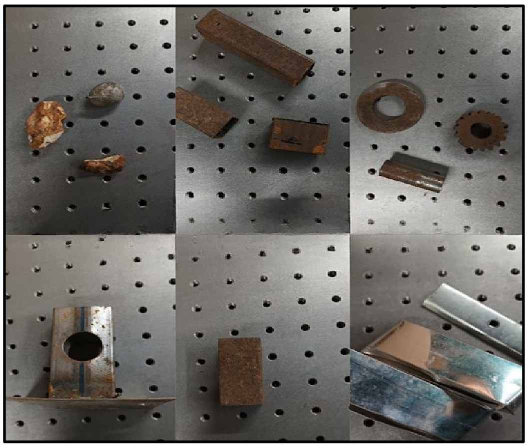

Figure 3: Debris Objects of Various Sizes and Shapes

The debris objects are of different shapes, sizes and materials. As shown in Figure 3, the various objects used are aluminium blocks, rings, rusted iron plates, stones of different shapes, etc. The pictures were captured utilizing a FLIR camera, which can capture both thermal and visible pictures, as seen in Figures 4A and 4B. Visible images taken using this camera in the experimental setup are presented in Figure 4A, whereas the thermal image taken in the experimental setup is shown in Figure 4B. The FLIR camera has a thermal mode and a visible spectrum mode. The visible spectrum camera has a resolution of 640 × 480p. The thermal camera can measure a range of temperatures from –20°C to +250°C.

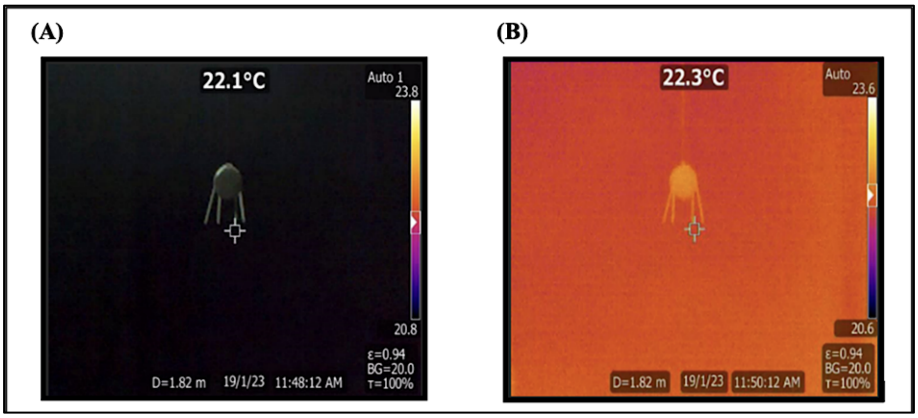

Figure 4: Images taken in the experimental setup. (A) Visible Image of Sputnik, (B) Thermal Image of Sputnik

However, the use of a FLIR camera to take visible and thermal images suffers from a major constraint due to differences in the focal points of these two lenses. The images captured have a slight shift in the position of the image in the visible and thermal spectra due to differences in the camera lens field of view for visible and thermal ranges. The resulting images from these lenses are displaced, as shown in Figures 5A and 5B. The visible image is presented in Figure 5A and the thermal image is shown in Figure 5B. This misalignment makes it difficult for the image fusion algorithm to produce accurate images. This challenge necessitates the use of image registration to align both images.

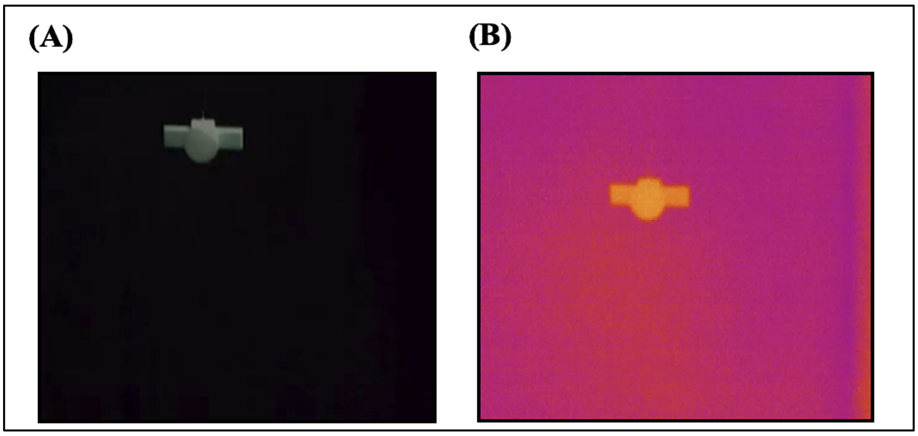

Figure 5: Visible and Thermal Images of Satellite1 Illustrating the Difference in Image Positions. (A) Visible Spectrum Image of Satellite1, (B) Simultaneously captured Thermal Image of Satellite1

Workflow 2

Space Environment Simulation: The subsequent second workflow includes the utilization of Blender. Blender is a free open-source 3D computer graphics software tool set utilized for synthesizing motion graphics, animations, special visualizations, visual effects, art, 3D models, VR, video games and interactive 3D applications.

The workflow for dataset creation in Blender follows multiple steps, as shown in the flowchart in Figure 6.

The first important step as illustrated in Figure 6 is to obtain satellite and debris models. The proposed dataset uses models from the NASA 3D resources repository (18). The model files from these repositories are converted into blend files and then imported to Blender. The simulations in Blender are made up of the following major components:

3D Models: The models were obtained from NASA's 3D model resources. A model is made up of collections consisting of various components of the objects and their properties. The model here is of the TESS satellite. It employs a variety of textures and components, such as shiny panels, gold foil, black crinkle, silver foil and so on.

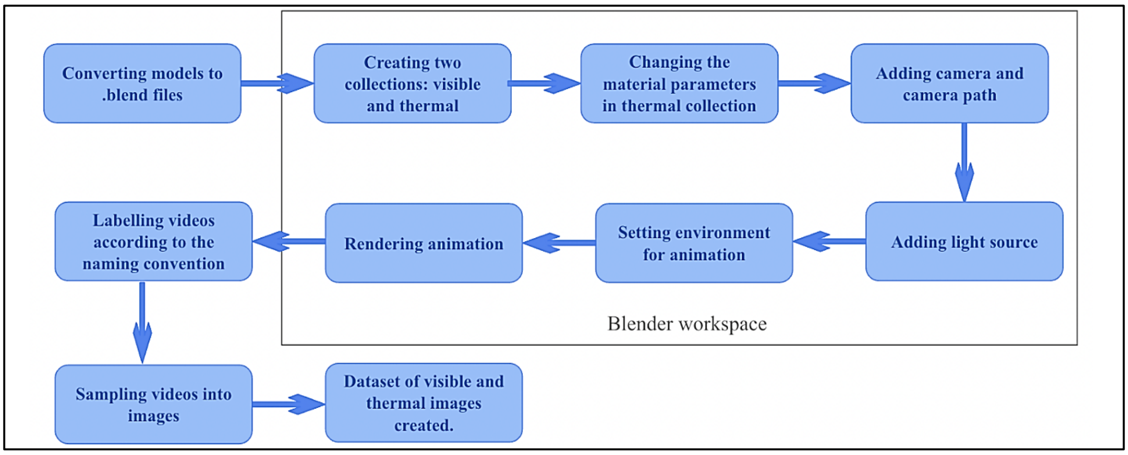

Figure 6: Workflow of Dataset Creation Using Blender

Camera: The camera revolves in a circular trajectory around the satellite, always facing it. This is required to create an animation of a satellite's visible and thermal views from various angles.

A sunlight source: It is used to illuminate the satellite from a specific direction. This comes in handy in the visible setup to change the light source strength to simulate the dark.

The next step involves creating two simultaneous collections of the model - a visible and a thermal collection. To obtain visible and thermal images, two different collections of materials are used on the satellite. In the visible collection, the materials used are the default ones that the 3D model came with. For the thermal collection, the materials have been developed for creating the thermal effect on satellite or debris objects. For developing a material of the thermal view, a Fresnel node, ColorRamp Node and Emission node are used to create the thermal imaging effect. Step 3 in Figure 6 illustrates this activity. The ColorRamp has a color variation set according to the temperature range of the FLIR camera palette (step 4). The color range varies for every object depending on the temperature parameters.

The next step is to add a light source to simulate the illumination conditions provided by the sun. The strength and direction of the light source are changed for different cases. The background color is set to black. Step 6 is to add a camera and then set a defined path to capture the animation of the simulation.

While rendering the animation, switching between the two sets of material collections and backgrounds obtains the required animations. The frames per second (fps) is set to 10 and the frame range is 100. As the camera moves along the same path around the satellite model, it captures the same angles for both visible and thermal images at the same instance of time.

To train the model on a wide range of illumination conditions, angles and thermal profiles, the parameters of the model were changed. This helps to simulate various conditions. The ones considered during dataset creation are: Temperature, Camera angle, Night-time, Zoom in/out.

Generating simulations using Blender suffers from a few limitations, such as models may not have individual parts separated as components in the collection. Due to this, it is not possible to change the material properties of those parts separately. Their material properties are the ones applied to the component they fall under in the hierarchy of the collection. Also, other complex space conditions such as solar storms and transitions are difficult to recreate in the simulation.

Data Pre-processing

Due to the misalignment in the images captured by the FLIR camera in the experimental setup, it was necessary to pre-process and align these images before performing image fusion. Image registration and image-to-map registration are preprocessing steps needed before performing image fusion and then image classification.

Image Registration: Due to the misalignment in the images captured by the FLIR camera in the experimental setup, it was necessary to process and align these images before performing image fusion. Image registration is one such technique used for pre-processing data. It is the process of aligning two or more images of the same scene captured at different times, from different perspectives, or using different sensors. Image registration addresses major image overlay issues, including rotation, scaling and skew distortions.

Several methods are commonly used for image registration, including feature-based and intensity-based methods, phase-correlation algorithms and the Iterative Closest Point (ICP) algorithm. Image registration can generally be implemented in two ways: Image-to-Map Registration and Image-to-Image Registration. Although both methods are used in the field of image registration, they refer to slightly different scenarios.

Image-to-Map Registration: Image-to-Map Registration is the process of correlating and aligning an image with a map or a geographic reference system. It involves determining the spatial transformation that maps the coordinates of the image to the corresponding locations on the map. The objective is to accurately overlay the image onto the map so that the geographic information contained in the image can be utilized or analyzed alongside the map data. This registration technique is widely used in satellite imaging, aerial photography and Geographic Information Systems (GIS).

Image-to-Image Registration: Image-to-Image Registration refers to the process of aligning multiple images with one another. It involves determining the transformation that best spatially aligns the images, typically by matching corresponding features or points within the images. The objective is to bring the images into a common coordinate system while minimizing geometric discrepancies or distortions between them. This method is extensively used in various applications such as medical imaging, remote sensing, computer vision and image analysis for tasks including image fusion, object tracking, image stitching and image comparison.

Image registration is generally performed in four major steps:

Feature Detection: In this step, distinctive features or key points are detected in each image. These features may include corners, edges, or other salient points that can be reliably identified. Feature detection algorithms aim to identify points that are invariant to changes in scale, rotation, lighting conditions and illumination.

Feature Matching: This step involves identifying corresponding features between the images by comparing the descriptors or characteristics of the detected features. Various matching algorithms, such as Nearest Neighbour and RANSAC (Random Sample Consensus), are employed to determine the best matches between features.

Transformation Model Estimation: Once the corresponding features are identified, the next step is to estimate the transformation model that maps one image onto another. Common transformation models include affine transformations, which involve translation, rotation, scaling and shearing, as well as projective transformations that account for perspective distortions. The transformation model is estimated using the matched feature pairs and is then used to align the images.

Image Resampling and Transformation: The final step in the image registration process is applying the computed transformation to one or both images. The resampling process involves mapping pixel values from the original image to their corresponding positions in the transformed image based on the estimated transformation parameters. Interpolation techniques are used to compute pixel values at non-integer coordinates.

Several feature matching algorithms are available for this purpose, including Features from Accelerated Segment Test (FAST), Scale-Invariant Feature Transform (SIFT), Harris Corner Detection, Speeded-Up Robust Features (SURF) and Oriented FAST and Rotated BRIEF (ORB) (19-22).

The proposed work implements a feature-based registration method based on the past research work (22). This approach assists in the detection and extraction of image features by combining filtering, edge detection and feature detection techniques. It also enables the matching of features between different images. Figure 7 illustrates the feature-based image registration method proposed in this work. The approach begins with image preprocessing, including filtering and edge detection, to enhance prominent structures and reduce noise. Distinctive features are then extracted using feature detection algorithms, enabling the identification of key points in both visible and thermal images. These corresponding features are subsequently matched to estimate the spatial transformation required for accurate alignment of the multimodal images.

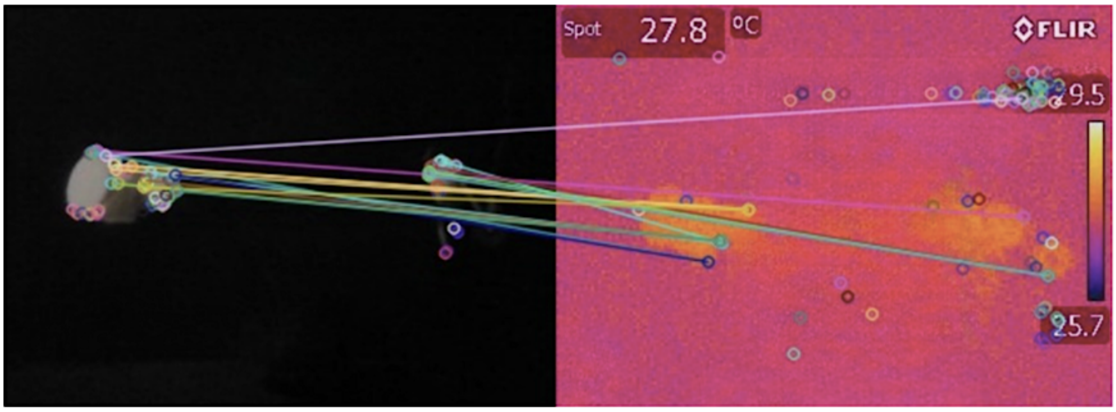

Figure 7: Feature Mapping in Image Registration, Corresponding Feature Points Identified in the Visible and Thermal Images are Matched to Establish Spatial Alignment Between the Two Modalities

Image Fusion

Image fusion is a technique that combines details and features from multiple source images into a single composite image. The primary objective of image fusion is to extract meaningful information and enhance the overall quality of the resulting image. The process involves merging images obtained from different sensors, such as thermal and visible imaging systems. Image fusion has numerous applications, including remote sensing, medical imaging, surveillance and computer vision. Various methodologies have been developed for image fusion, such as pixel-based fusion and feature-based fusion techniques. Each method possesses its own advantages and limitations. The selection of a fusion technique depends on the specific application requirements and the characteristics of the input images. Different methodologies offer trade-offs between simplicity, computational efficiency, detail preservation and overall performance.

In this research, two different methodologies for the fusion of visible and thermal images were explored.

Using Guided Filtering and Two-scale Image Reconstruction: This algorithm follows a two-step process. Initially, it performs a two-scale decomposition on the input images, separating them into base and detail layers. The base layer represents the coarse-scale structure and global information, while the detail layer captures fine-scale details and local features. This decomposition helps preserve important information and enhances the quality of the fused image. Subsequently, guided filtering is applied separately to the base and detail layers. Guided filtering utilizes a guidance image, which may be one of the input images or an additional reference image, to direct the filtering process. This approach effectively smooths the base and detail layers while preserving edges and structures according to the guidance image. By adaptively adjusting the filtering parameters, the guided filtering process aligns and combines information from the input images in a controlled manner. Finally, the filtered base and detail layers are combined to produce the fused image. The base layers from the input images are weighted and averaged according to their importance and contribution. Similarly, the detail layers are fused using a weighted averaging approach based on their relevance and significance. The resulting fused image is visually informative and integrates salient features from the input images while maintaining spatial consistency and preserving details.

Using Laplacian Pyramid Decomposition for Weight Map Creation: In this approach, the input images are first decomposed into Laplacian pyramids consisting of a sequence of band-pass filtered images at different scales. The pyramid decomposition separates the images into different frequency bands, enabling more precise image fusion. To determine the contribution of each pixel from the input images to the final fused image, weight maps are generated by analyzing the Laplacian pyramids. These weight maps emphasize regions with high saliency or importance within each image. Various techniques, such as local contrast analysis, gradient magnitude computation and entropy measures, can be used to generate the weight maps. These maps effectively capture distinctive features and important information present in each source image. Once the weight maps are generated, the fused image is reconstructed by combining the weighted Laplacian pyramids. Pixels associated with higher weights contribute more significantly to the final image, ensuring the preservation of important details. By utilizing Laplacian pyramid decomposition and weight maps, this method enables seamless integration of multiple images while emphasizing the most relevant information.

These algorithms as well suffer from a few limitations such as they are unable to generate informative fused images when the visible images are significantly dark, intermediate processing operations modify the RGB values of the images while producing the fused outputs and there is a significant loss of detail and edge information.

Proposed Two-Step Fusion Method: To address these limitations, a novel Two-Step Image Fusion algorithm for visible and thermal image fusion has been proposed. The proposed algorithm performs efficiently on the generated dataset while preserving edge details. It is also effective for fusing visible and thermal image pairs where the visible image contains minimal information. The method utilizes a Laplacian kernel to preserve important details from the source images.

The Laplacian kernel, also known as the Laplacian filter or Laplacian operator, is widely used for edge detection and image sharpening. It is a convolutional kernel applied to an image to highlight regions with rapid intensity variations, which typically correspond to edges or boundaries between objects and regions within the image. The Laplacian operator computes the second derivative of image intensity at each pixel location. By convolving the kernel with the image, high-frequency components are enhanced, thereby emphasizing transitions in intensity values and facilitating edge detection. The Laplacian kernel is designed to capture both vertical and horizontal intensity variations, enabling the detection of edges in all directions. It is particularly effective for detecting edges with variations in both intensity and orientation.

In addition to edge detection, the Laplacian kernel can also be used for image sharpening. By subtracting the Laplacian-filtered image from the original image, high-frequency components are amplified, resulting in a sharpened image with enhanced details. Overall, the Laplacian kernel is a powerful image processing tool for edge detection, image sharpening and image enhancement, supporting applications such as object detection, segmentation and feature extraction.

The proposed algorithm consists of a two-step process. Initially, a pair of visible and thermal images is fused together. Subsequently, a sharpened-edge image is generated using the Laplacian kernel. Finally, this sharpened image is fused with the initially fused visible-thermal image. Thus, the fusion method is applied twice: first to the visible-thermal image pair and then to the resulting fused image along with the sharpened-edge image.

The 2-Step Image Fusion Algorithm is as follows:

Load the corresponding visible and thermal images as input images.

Define a fusion function that combines two images according to specified weights.

- Resize the images and convert them to a floating-point data type.
- Fuse the images by multiplying them with their respective weights.
- Normalize the pixel values to bring them to a suitable scale.
- Return the fused image.

Call the fusion function and pass the thermal and visible images with equal weights of 0.5.

Generate a sharpened-edge image using the Laplacian kernel.

Call the fusion function again and pass the previously fused image and the sharpened-edge image with weights of 0.8 and 0.2, respectively.

Save the final fused image obtained.

Equations [1-4] describe the mathematical representation of how each image matrix is fused in the proposed approach. These equations mathematically represent the fusion of visible spectrum and thermal images, the use of the Laplacian filter to extract boundaries, the combination of the fused image with the boundaries and the generation of a higher quality final image. Equation [1] represents the Laplacian kernel used for edge detection in image processing.

It indicates the regions where there is a sudden change in intensity. These sudden changes may correspond to boundaries, edges or sometimes a few fine details in the image. It is used in the current work to preserve and enhance edge details from the fused visible and thermal images.

$$K = ([0, -1, 0], [-1, 4 ,-1], [0, -1, 0]) \quad [1]$$

Equation [2] describes the combining of thermal parameters and visible spectrum parameters into a single image. A simple weighted-average fusion process where both modalities contribute equally. This equation creates an intermediate fused image by combining $I_{thermal}$ and $I_{visible}$ with equal weights of 0.5 each.

$$I_{intermediate} = 0.5 * (I_{thermal} + I_{visible}) \quad [2]$$

Equation [3] performs a convolution between the intermediate fused image $I_{intermediate}(x+i, y+j)$ and the Laplacian kernel K(i, j), which creates an enhanced fused image. This preserves the structural and edge information in the fused image, which might otherwise be lost during image fusion process.

$$I_{edges}(x, y) = \sum_{i,j}[I_{intermediate}(x+i, y+j) * K(i, j)] \quad [3]$$

Equation [4] indicates how the final fused image is obtained by combining the visible image, the thermal image and the extracted boundary details.

$$I_{fused} = 0.4 * (I_{visible} + I_{thermal}) + 0.2 * edges \quad [4]$$

Sample visible and corresponding thermal images from the created dataset are shown in Figure 8. Figure 8A presents debris object models generated using Blender, while Figure 8B shows visible and corresponding thermal images of satellites. The images demonstrate that visible images captured under dark, unilluminated conditions contain limited visual information, with only object edges and boundaries being discernible. In contrast, the corresponding thermal images clearly reveal the structure of the object.

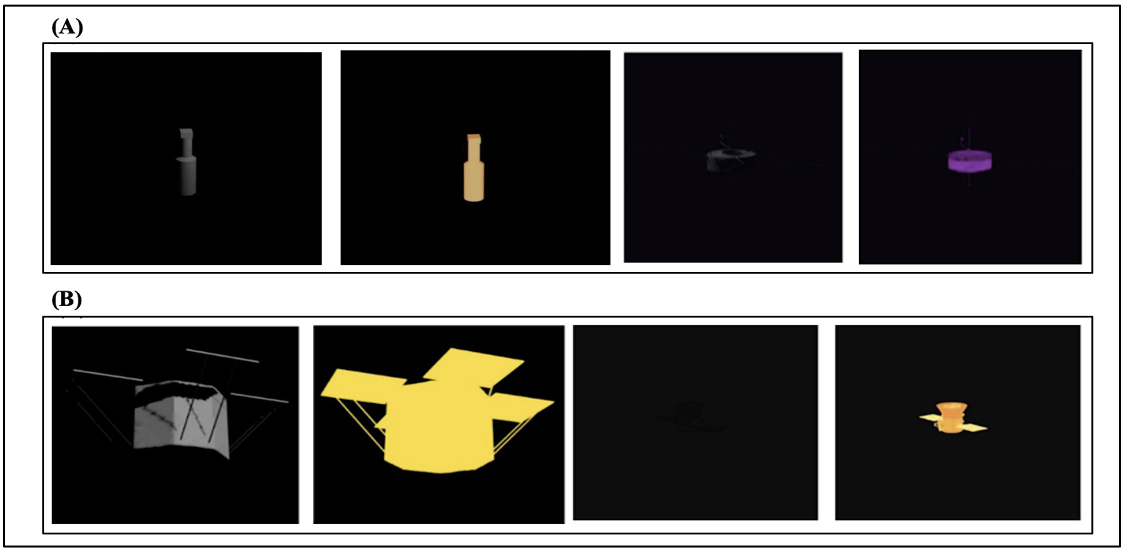

Figure 8: Sample Images of Debris and Satellites in the Dataset. (A) Visible and Corresponding Thermal Images of Two Debris Models from the Dataset, (B) Visible and corresponding Thermal Images of Two Satellite Models from the Dataset

By combining the visible and thermal images at the base and detail layers using the proposed two-step fusion algorithm, a more comprehensive and informative fused image is obtained. The enhanced fused image improves the accuracy of subsequent classification, enabling more reliable discrimination between debris and satellites.

Figure 9 shows image fusion using the proposed two-step image fusion algorithm described above. Figure 9A shows the visible image of a satellite object, Figure 9B shows the thermal image of the same object in an unilluminated or dark state and Figure 9C presents the fused image of the same satellite object. It can be observed from the fused image that, even under dark or low-illumination conditions, important image features are effectively preserved and enhanced. This improved feature visibility facilitates more accurate and reliable classification of space objects in subsequent processing stages.

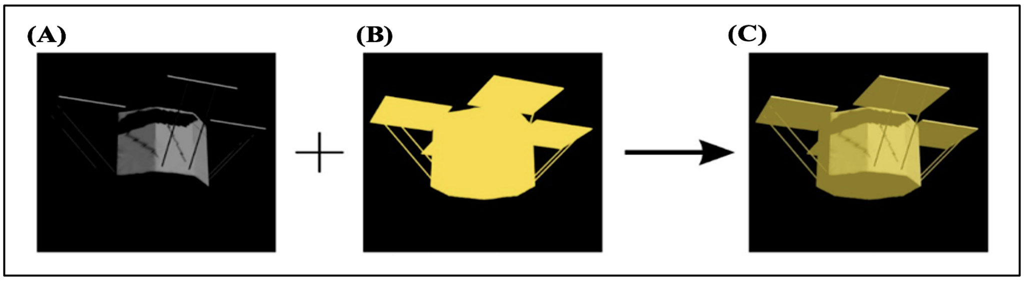

Figure 9: Image Fusion using the proposed two step Image Fusion Algorithm. (A) Visible Image of a Satellite Object, (B) Thermal Image of the same Satellite in the Un-illuminated or dark state, (C) Fused Image of the same Satellite Object

Image Classification

The process of classifying objects into predefined labels is termed classification. In this case, fused images of space objects are classified as either space debris or satellites. Deep neural networks have been used for classification purposes. The model learns from the training and validation sets present in the dataset.

For easier model definition and reduced training time, pre-trained networks are used. Powerful pre-trained networks ensure that relevant features are extracted from the images to make predictions on unseen images. Accurate and efficient image classification of space objects is of utmost importance for enabling effective space situational awareness, collision avoidance and the overall safety and sustainability of space operations. Some widely used pre-trained models, such as VGG, ResNet, DenseNet, GoogLeNet and InceptionV3, have been implemented for classification purposes (23-27).

For the implementation of the classification model, the Python programming language, along with the PyTorch, Matplotlib and Pandas libraries, were used. The algorithm used to classify objects using pre-trained networks is given below. It provides a brief overview of how the core logic of the classification model was implemented. To ensure that the models are not overfitted to the dataset, the images used for training have been separated from those used for validation and testing. Ensuring that various angles and conditions of the same satellite or debris model are covered helps the classification model train on more features and improves its generalization capability.

Algorithm

```
Import Dataset using ImageFolder Function in pytorch
Create DataLoader objects containing batches of images using DataLoader functionality in PyTorch
Move the DataLoaders to GPU
function accuracy (output, labels)
    prediction = maximum(output_probability)
    accuracy = correct_prediction / total prediction
Define functions in a Base Class that implements nn.Module class
    function training(batch)
        generate predictions
        calculate cross entropy loss
    function validation(batch)
        generate predictions
        calculate cross entropy loss
        calculate accuracy
    function epoch_end(output, epoch, result)
        calculate training loss, validation loss, validation accuracy
Import pre-trained model and replace last layer with fully connected layer having output size=2
```

```
function fit(epochs, lr, model, train_dataloader, validation_dataloader, optim_function)
for each epoch
    train the model
    calculate loss per batch
    adjust weights
Calculate validation loss
Initialize and load model to the GPU
fit()
Predict accuracy on test data loader
Log metrics as graphs
Save model as model.pth, to use the weights for future use
```

Challenges Faced

While developing a solution for the space debris identification problem, there were many challenges involved in starting from dataset creation to image fusion, as well as in image classification.

Challenges in Dataset Creation: In the experimental setup, the offset between the positions of the thermal and visible lenses in the FLIR camera caused displacement between the thermal and visible images obtained from them. This created difficulties during the image-fusion process. While using Blender 3D for dataset generation, accurate simulations of space conditions could not be achieved. There was also a lack of availability of compatible models in accessible repositories. Furthermore, simulating complex space conditions and their effects on space objects proved to be complicated in Blender.

Challenges in Data Preprocessing: The drawbacks mentioned in Section 4.1(a) led to the use of image-registration techniques to address the alignment problem. The task involved identifying key points and descriptors in the visible and thermal images and aligning them accordingly. However, in many cases, the visible images were partially or completely covered in darkness, causing key points to remain undetected. As a result, distorted images were produced while mapping them to the thermal images. This eventually led to the discontinuation of Workflow 1.

Challenges in Image Fusion: The existing image-fusion algorithms did not produce optimal results under dark visible-image conditions for the fusion of thermal and visible-image datasets. The fusion operations modified the input images and therefore produced varying results for different application scenarios. Additionally, the existing algorithms resulted in a significant loss of detail and edge information. To overcome this issue, a new algorithm was developed that fused the images with equal weights while preserving edge details.

Challenges in Image Classification: Initially, the classification model overfitted to the images present in the dataset, which did not ensure good generalization in real-world scenarios. To address this issue, greater diversity was introduced into the dataset. New space objects were specifically added to the validation and testing datasets, ensuring that the testing data remained unseen by the classification model during training.

Results and Discussion

Various pre-trained deep learning models, including VGG, ResNet, DenseNet, GoogLeNet and InceptionV3, were evaluated for the classification of fused satellite and debris images. The dataset was divided into training, validation and testing subsets to ensure reliable model evaluation and minimize overfitting. Table 1 summarizes the performance of the investigated models under the selected hyperparameter settings.

Initially, a CNN architecture with a 64 × 64 × 128 configuration was trained using the laboratory dataset. The model achieved an overall classification accuracy of approximately 50% on unseen test samples, indicating limited discriminative capability for the dataset under consideration.

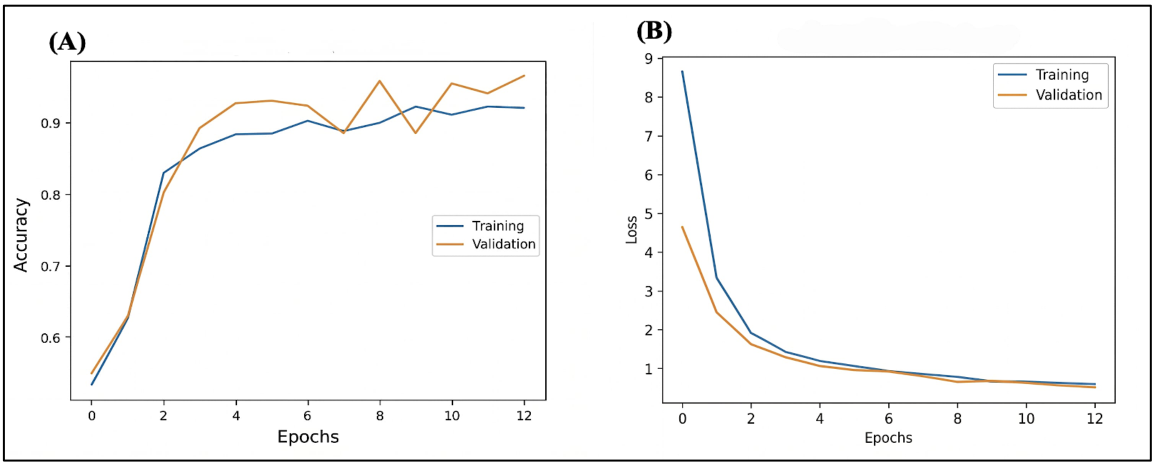

Figure 10: Training and Validation Accuracy and Loss Curves for the CNN model (64 x 64 x 128). (A) Training and Validation Accuracy Curves Plotted Against Epochs, (B) Training and Validation Loss Curves Plotted Against Epochs

The corresponding classification report showed precision values of 57% and 41% for the satellite and debris classes, respectively, while the recall values were 58% and 41%. The resulting F1-scores of 57% for satellites and 41% for debris further confirm the challenges associated with accurately distinguishing between the two classes using the basic CNN architecture. These results suggest that more advanced deep learning models are required to effectively extract representative features from the fused images and improve classification performance.

Figure 10 presents the training and validation performance of the CNN model with an input size of 64 × 64 × 128. Figure 10A shows the accuracy curves for the training and validation datasets across successive epochs, illustrating the model's learning progression and convergence. Figure 10B presents the corresponding training and validation loss curves, demonstrating the reduction in prediction error during the training process and providing insight into the model's generalization capability.

The relatively low performance of the baseline CNN model highlights the complexity of the space object classification problem. Recent studies have reported improved recognition accuracy using deeper architectures and multimodal feature extraction techniques for spacecraft and debris recognition. Similarly, RGB-D and multimodal deep learning approaches have demonstrated superior classification performance by leveraging complemen-tary information from multiple sensing modalities (12). These findings support the use of deeper pre-trained networks and fused imaging data for enhanced space object classification. Similar observations have been reported in recent studies employing multimodal sensing and deep learning techniques for space object classification (12, 24, 27)

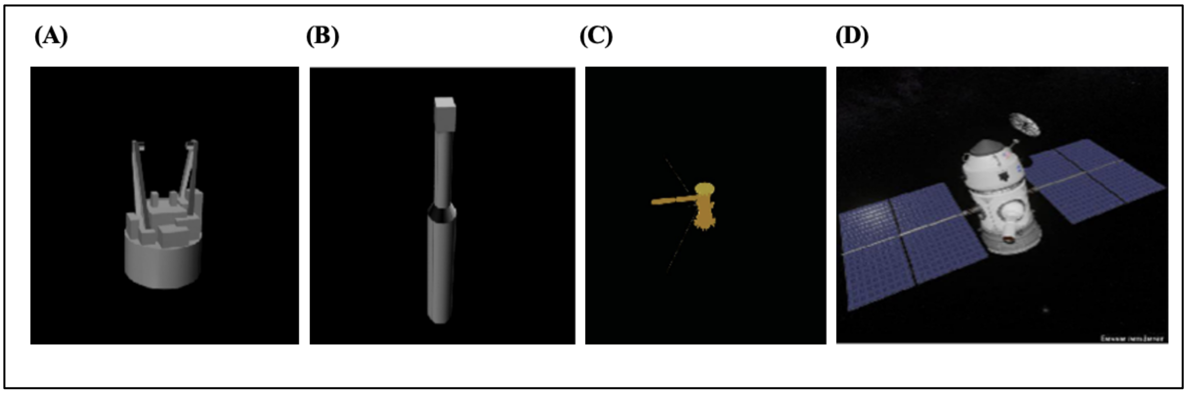

Figure 11: Debris and Satellite Image Prediction using the CNN. (A) Predicted Class: Debris, Confidence: 0.95, (B) Predicted Class: Debris, Confidence: 0.96, (C) Predicted Class: Satellite, Confidence: 0.95 and (D) Predicted Class: Satellite, Confidence: 0.95

Figure 11 presents examples of debris and satellite images correctly classified by the CNN model. The images were generated using 3D-printed models captured through the experimental setup or synthetic models created in Blender. Figures 11A and 11B were classified as debris, with confidence scores of 0.95 and 0.96, respectively, while Figures 11C and 11D were classified as satellites, with confidence scores of 0.95 each. The model achieved high prediction confidence, demonstrating its effectiveness in distinguishing between debris and satellites.

The ResNet50 model was employed to classify objects as satellites or debris using the synthetically generated Blender dataset. By optimizing the learning rate, the model achieved an overall classification accuracy of 97.52%. Evaluation was performed on previously unseen test objects, demonstrating the model's ability to generalize effectively. Figure 12 presents the training and validation accuracy and loss curves for the ResNet50 model, where the x-axis represents the training epochs and the y-axis represents the accuracy and loss in the respective plots. Figure 12A shows the training and validation accuracy curves plotted against epochs, while Figure 12B presents the corresponding training and validation loss curves.

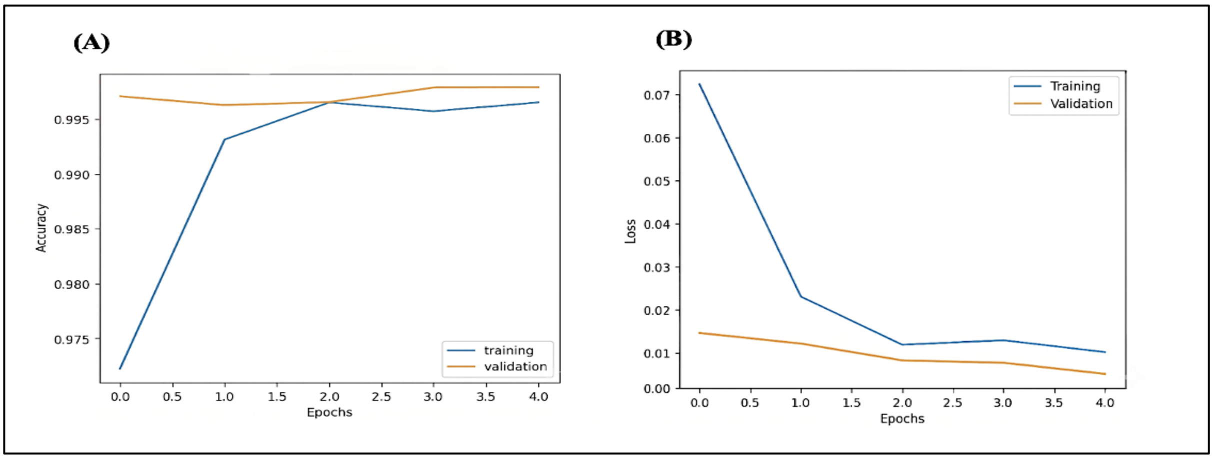

Figure 12: Training and Validation Accuracy and Loss Curves for the ResNet 50 model. (A) Training and Validation Accuracy versus Epochs, (B) Training and Validation Loss versus epochs

The model correctly classified the test samples with confidence scores of approximately 95%, indicating robust classification performance. The high classification accuracy achieved by the ResNet50 demonstrates the effectiveness of deep learning in extracting discriminative features from fused visible and thermal images. The close agreement between the training and validation curves, as presented in Figure 12, indicates stable convergence, suggesting that the model generalized well to unseen data. These findings are consistent with recent studies that have reported improved spacecraft and debris recognition using deep learning and multimodal data representations (12). The results obtained in this study further support the use of image fusion combined with deep networks for accurate space-object classification.

Similarly, the other deep learning models were implemented on the combined dataset comprising images acquired from the dark-room experimental setup and images synthetically generated using Blender. Table 1 summarizes the performance of ResNet50, ResNet101, DenseNet201, DenseNet169, GoogLeNet, VGG16, VGG19 and InceptionV3 in terms of precision, accuracy and F1-score. Among the evaluated architectures, GoogLeNet achieved the highest performance, with a precision of 0.999, an accuracy of 100% and an F1-score of 0.999. ResNet50 and InceptionV3 also demonstrated excellent classification performance, with precision values exceeding 0.97 and 0.99, respectively. In contrast, DenseNet201 and the VGG-based models exhibited comparatively lower performance, indicating a reduced ability to discriminate between the satellite and debris classes in the fused image dataset.

The superior performance of GoogLeNet may be attributed to its inception modules, which enable the extraction of multi-scale features while maintaining computational efficiency. The results suggest that the fused visible–thermal images preserve complementary structural and thermal characteristics that can be effectively exploited by deep architectures for accurate object classification.

Similar findings have been reported in recent studies, where multimodal sensing and deep learning approaches significantly improved spacecraft and debris recognition performance by leveraging complementary information from different imaging modalities (12). The consistently high performance achieved by GoogLeNet, ResNet50 and InceptionV3 further demonstrates that the proposed image-fusion framework enhances feature representation and improves the discrimination of space-resident objects under varying imaging conditions.

The observed performance trends are consistent with previous studies that have demonstrated the effectiveness of deep learning models trained on realistic synthetic datasets for space-object recognition and classification (6, 8).

Table 1: Results of Classification Models

Models	Precision	Accuracy	F1-score
VGG16	0.533	53.353	0.533
DenseNet 201	0.756	75.685	0.756
DenseNet 169	0.921	92.187	0.921
ResNet 50	0.975	97.522	0.975
ResNet 101	0.945	94.596	0.945
Inception v3	0.998	99.847	0.998
GoogLeNet	**0.999**	**100**	**0.999**

Table 2 presents a comparison between classification performance using visible images alone and fused visible–thermal images. The fused images achieved a precision of 0.999, an accuracy of 100% and an F1-score of 0.999, substantially outperforming the visible-image dataset, which achieved a precision of 0.515, an accuracy of 51.50% and an F1-score of 0.515. The marked improvement demonstrates the effectiveness of the proposed image-fusion framework in enhancing object identification and improving satellites-debris classification.

Table 2: Comparison of Classification Results for the Visible-Image Dataset and the Fused Thermal–visible Image Dataset

Model	Precision	Accuracy	F1 – score
GoogLeNet (Visible)	0.515	51.5	0.515
GoogLeNet (Fused)	**0.999**	**100**	**0.999**

The superior performance of the fused images can be attributed to the complementary nature of the visible and thermal modalities. While visible images provide detailed structural, textural and edge information, thermal images capture object signatures even under poor illumination conditions. The fusion process combines these complementary features into a single informative representation, enabling the deep learning models to extract more discriminative features and reduce classification ambiguity.

Similar benefits of integrating visible and infrared information have been reported in image-fusion studies, where fused images consistently improved object detection and recognition performance compared with single-modality inputs (2, 4).

Collectively, these results validate the effectiveness of the proposed fusion and classification framework, demonstrating its capability to improve space-object recognition accuracy and supporting its application in automated space debris detection and space situational awareness systems.

Conclusion

Space debris particles pose a significant risk to functioning satellites and spacecraft in space. The exponential increase in the number of satellites and space debris presents major challenges to future space missions. Effective detection and categorization of space debris have become an essential activity for ensuring the safety and sustainability of space-based operations.

In this context, this paper presents a fusion and classification technique that addresses the issue of effective detection and classification of space debris and operational satellites. The space debris can be of different shapes, sizes and materials.

However, as the images of space debris are not available anywhere, it was necessary to create a dataset of images closely resembling space debris. This was achieved by creating a dataset of visible and thermal images of satellites as well as debris, which can be fused for developing a classification model that takes the fused images as input for detecting Space Debris and Satellites. Dataset creation was divided into two separate workflows. In the first stage, an experimental setup was created by setting up a visible-spectrum camera and a thermal camera in the dark-room setup for data creation. In the second stage, the simulation of the same setup is created using Blender software to render animations and create a dataset of visible and thermal images. Around 12,000 such images of Debris and Satellite (thermal + visible) were created and used to train the deep learning models to identify two classes: Satellite class and Debris class.

The images captured in the dark room experimental setup were preprocessed for further fusion of visible and thermal images. The image fusion with the guided filtering method was applied to the generated dataset. To correct the positional error in the fused images, SURF and ORB approaches were used. For the images generated using Blender setup, a two-step image-fusion algorithm is implemented. It used a Laplacian filter for preserving the details from the source images. A convolutional kernel was applied to an image to highlight regions of rapid intensity change. The two-step Image Fusion algorithm provided the ability to find key points and descriptors in the visible images which had a significant amount of darkness.

From the comparison between using a dataset of visible images and fused images, a significant difference was observed in the performance between the two types of image data. The fused images exhibited better performance with a precision of 0.999, accuracy of 100% and F1-score of 0.999. These scores indicate near-perfect classification results, suggesting that the fusion of visible and thermal data sources significantly enhances the model's accuracy and ability to distinguish between classes.

The results highlight the importance of image fusion in improving the classification performance. By combining different data sources or modalities such as visible and thermal images, the model has significantly enhanced the effectiveness of image classification tasks leading to improved accuracy.

Thus, the proposed research work can assist in real-time monitoring and identification of objects encountered by the spacecraft during spacecraft missions. This information can be used to make informed decisions regarding course corrections or potential collision avoidance measures. Moreover, the fused image classification model can enhance satellite imagery analysis by providing additional information from both visible and thermal domains. It can assist in identifying specific features or anomalies related to space debris or satellites, enabling more accurate analysis and interpretation of satellite imagery.

Future Work

The models used in this paper performed binary classification. Future scope of this paper could be a model performing multi-class classification. Additional features could be considered for classification. Further, these models could be tested on real time data. And lastly, motion of space objects can be considered for classification of space objects, thus incorporating video fusion techniques.

Some possible application areas of the proposed approach of using thermal and visible image fusion in order to detect space objects can be, space surveillance and monitoring, space debris mitigation, satellite imagery analysis and research and exploration missions by facilitating the identification and study of space debris and satellites. It can contribute to the understanding of space environment dynamics, orbital debris distribution and the behaviour of functioning satellites.

Abbreviations

None.

Acknowledgement

This work was supported by the U. R. Rao Satellite Center (URSC), Indian Space Research Organisation (ISRO), Bengaluru through the ISRO-SPPU Space Technology Cell, Savitribai Phule Pune University (Project 198). We thank the scientists at URSC, ISRO Bengaluru, for their continuous guidance and support. We are also grateful to the Principal and all our colleagues from Cummins College of Engineering for Women, Pune, India who supported us while working on this project.

Author Contributions

Sunita Jahirabadkar: Conceptualization, Study Design, Data Collection, Data Analysis, Interpretation of the Results, Critical Revision of the Manuscript, Approval the Final Version of the Manuscript, Raahi Kadu: Literature Review, Methodology Development, Data Analysis, Implementation, Algorithm Testing, Manuscript Preparation, Sai Gokhale: Literature Review, Methodology Development, Data Analysis, Implementation, Algorithm Testing, Manuscript Preparation, Grishma Deshmukh: Literature Review, Methodology Development, Data Analysis, Implementation, Algorithm Testing, Manuscript Preparation, Sejal Chaudhari: Literature Review, Methodology Development, Data Analysis, Implementation, Algorithm Testing, Manuscript Preparation, Aditya R: Conceptualization, Study Design, Data Collection, Data Analysis, Interpretation of the Results, Critical Revision of the Manuscript, Approval the Final Version of the Manuscript. All authors have read and approved the submitted manuscript and agree to be accountable for all aspects of the work.

Conflict of Interest

All authors declare that there are no apparent or actual conflicts of interest related to this work, including financial, personal, academic, or institutional relationships that could inappropriately influence the study or its interpretation.

Data Availability

The datasets used in this study are publicly available from the respective sources cited in the manuscript.

Declaration of Artificial Intelligence (AI) Assistance

While preparing this paper, the authors used AI-assisted technologies and generative AI for removing grammatical errors and making the paper more readable. The authors carefully reviewed and edited the generated content and take full responsibility for the accuracy, originality and integrity of the final manuscript. No AI tools were used for data analysis, result generation, or scientific interpretation.

Ethics Approval

Ethical approval was not required for this study as it did not involve human participants or animal subjects.

Funding

This work is funded and supported by U. R. Rao Satellite Center (URSC), Indian Space Research Organization (ISRO), Bengaluru through the ISRO-SPPU Space Technology Cell, Savitribai Phule Pune University (Project 198).

References

1. Haridim M, Shaked A, Cohen N, Gavan J. Challenges of space debris detection, tracking and monitoring in near-Earth orbit: overview of current status and mitigation strategies. Information. 2026;17(3):253. doi:10.3390/info17030253
2. Ma J, Ma Y, Li C. Infrared and visible image fusion methods and applications: a survey. Information Fusion. 2019;45:153-78. 45:153-178. doi:10.1016/j.inffus.2018.02.004
3. Jiang T, Cao Y, Ding M, Zhang Z. Visible and infrared image fusion for space debris recognition with convolutional sparse representation. In: Proceedings of the IEEE CSAA Guidance, Navigation and Control Conference (CGNCC); 2018. https://doi.org/10.1109/GNCC42960.2018.9019121
4. Xiang X, Zhou G, Niu B, Pan Z, Huang L, Li W, Wen Z, Qi J, Gao W. Infrared-visible image fusion meets object detection: towards unified optimization for multimodal perception. Remote Sens.2025;17(21): 3637. doi:10.3390/rs17213637
5. Dawson JA, Bankston CT. Space debris characterization using thermal imaging systems. In: Proceedings of the Advanced Maui Optical and Space Surveillance Technologies Conference; 2010;14-17. https://amostech.com/TechnicalPapers/2010/Systems/Dawson.pdf
6. Zhang Z, Deng C, Deng Z. A diverse space target dataset with multidebris and realistic on-orbit environment. IEEE J Sel Top Appl Earth Obs Remote Sens. 2022;1-14. doi:10.1109/JSTARS.2022.3203042
7. Xi J, Xiang Y, Ersoy OK, Cong M, Wei X, Gu J. Space debris detection using feature learning of candidate regions in optical image sequences. IEEE Access. 2020;8:150864-77. doi:10.1109/ACCESS.2020.3016761
8. Perez M, Mohamed Ali MA, Garcia Sanchez A, *et al.* Detection and identification of on-orbit objects using machine learning. In: Proceedings of the 8th European Conference on Space Debris. 2021;8(1). http://hdl.handle.net/10993/48796
9. Rodin CD, de Lima LN, de Alcantara Andrade FA, Haddad DB, Johansen TA, Storvold R. Object classification in thermal images using convolutional neural networks for search and rescue missions with unmanned aerial systems. International Joint

Conference on Neural Networks (IJCNN). 2018:1-8. doi:10.1109/IJCNN.2018.8489465
10. Jiang C, Ren H, Ye X, Zhu J, Zeng H, Nan Y, Sun M, Ren X, Huo H. Object detection from UAV thermal infrared images and videos using YOLO models. International Journal of Applied Earth Observation and Geoinformation. 2022;112:102912. doi:10.1016/j.jag.2022.102912
11. Chaudhary S, Jain P, Jakhetiya V, Guntuku SC, Subudhi BN. Localizing features with masking for satellite and debris classification. IEEE International Conference on Image Processing Challenges (ICIPC). 2021;16-20. doi:10.1109/ICIPC53495.2021.9620178
12. AlDahoul N, Karim HA, Momo MA. RGB-D based multi-modal deep learning for spacecraft and debris recognition. Sci Rep. 2022;12(1):3924. doi:10.1038/s41598-022-07846-5
13. Salvatore N, Fletcher J. Learned event-based visual perception for improved space object detection. In: Proceedings of the IEEE/CVF Winter Conference on Applications of Computer Vision (WACV); 2022; 2888-97. doi:10.1109/WACV51458.2022.00336
14. Musallam MA, Gaudilliere V, Ghorbel E, Al Ismaeil K, Perez MD, Poucet M, Aouada D. SPARK: pacecraft recognition leveraging knowledge of space environment: Simulator, dataset, competition design and analysis. In2021 IEEE International Conference on Image Processing Challenges (ICIPC) 2021 Sep 19:11-5. doi:10.48550/arXiv.2104.05978
15. Zhang C, Guo B, Liao N, Zhong Q, Liu H, Li C, Gong J. STAR-24K: a public dataset for space common target detection. KSII Trans Internet Inf Syst. 2011;16(2):365-80. doi:10.3837/tiis.2022.02.001
16. Murray J, Kennedy T, Matney M, Miller R. Radar observations from the Haystack ultrawideband satellite imaging radar in 2019. 8th European Conference on Space Debris. 2021. https://conference.sdo.esoc.esa.int/proceedings/sdc8/paper/169/SDC8-paper169.pdf
17. Theodorou I, Ilioudis C, Clemente C, Vasile M, Soraghan J. SISAR imaging for space debris based on nanosatellites. IET Radar Sonar Navig. 2020;14(8): 1192-1201. doi:10.1049/iet-rsn.2019.0574
18. National Aeronautics and Space Administration. 3D Resources [Internet]. NASA Science. 2026 Apr 13. https://science.nasa.gov/3d-resources/
19. Trajkovic M, Hedley M. Fast corner detection. Image Vis Comput. 1998;16(2):75-87. doi:10.1016/S0262-8856(97)00056-5
20. Yi-Bo L, Jun-Jun L. Harris corner detection algorithm based on improved contourlet transform. Procedia Eng. 2011;15:2239-43. doi:10.1016/j.proeng.2011.08.419
21. Bay H, Tuytelaars T, Van Gool L. SURF: Speeded Up Robust Features. Computer Vision – ECCV 2006. 2006;404-17. https://doi.org/10.1007/11744023_32
22. Rublee E, Rabaud V, Konolige K, Bradski G. ORB: An efficient alternative to SIFT or SURF. IEEE International Conference on Computer Vision (ICCV). 2011;2564-2571. doi:10.1109/ICCV.2011.6126544
23. Simonyan K, Zisserman A. Very deep convolutional networks for large-scale image recognition. arXiv [Preprint]. 2014. doi:10.48550/arXiv.1409.1556
24. He K, Zhang X, Ren S, Sun J. Deep residual learning for image recognition. IEEE Conference on Computer Vision and Pattern Recognition (CVPR). 2016;770-8. doi:10.1109/CVPR.2016.90.
25. Huang G, Liu Z, Van Der Maaten L, Weinberger KQ. Densely connected convolutional networks IEEE Conference on Computer Vision and Pattern Recognition (CVPR). 2017;4700-08. doi:10.1109/CVPR.2017.243
26. Szegedy C, Liu W, Jia Y, Sermanet P, Reed SE, Anguelov D, Erhan D, Vanhoucke V, Rabinovich A. Going deeper with convolutions. IEEE Conference on Computer Vision and Pattern Recognition (CVPR); 2015;1-9. doi:10.1109/CVPR.2015.7298594
27. Szegedy C, Vanhoucke V, Ioffe S, Shlens J, Wojna Z. Rethinking the Inception architecture for computer vision IEEE Conference on Computer Vision and Pattern Recognition (CVPR). 2016;2818-2826. doi:10.1109/CVPR.2016.308

How to Cite: Jahirabadkar S, Kadu R, Gokhale S, Deshmukh G, Chaudhari S, Aditya R. Seeing Through Darkness: Fusion of Optical and Thermal Features for Improved Space Object Classification. Int Res J Multidiscip Scope. 2026;7(3):1091-1108. DOI: 10.47857/irjms.2026.v07i03.012212